IEEE Access
Multidisciplinary | Rapid Review | Open Access Journal

Received December 3, 2020, accepted December 28, 2020, date of publication January 1, 2021, date of current version January 14, 2021.

Digital Object Identifier 10.1109/ACCESS.2020.3048695

Gradient Descent Optimization-Based SINS Self-Alignment Method and Error Analysis

JINGCHUN LI[1], JIACHONG CHANG[2], AND YA ZHANG[2]
[1]Peng Cheng Laboratory, Shenzhen 518000, China
[2]School of Instrumentation Science and Engineering, Harbin Institute of Technology, Harbin 150001, China

Corresponding author: Jingchun Li (ljc150001@163.com)

This work was supported in part by the National Natural Science Foundation of China under Grant 51509063, Grant 51709068, and Grant 91948204; in part by the China Postdoctoral Science Foundation under Grant 2020M682824; in part by the National Key Research and Development Program of China under Grant 2017YFB0503001; and in part by the Fundamental Research Funds for the Central Universities under Grant HIT.NSRIF.201813.

ABSTRACT In this paper, the self-alignment for stationary strapdown inertial navigation system (SINS) is formulated as an optimization problem, and two gradient descent optimization-based SINS self-alignment methods (GD1 and GD2) are proposed. The highlight lies in that two quaternion-based objective functions are firstly formulated to solve the stationary SINS self-alignment problem. Different from conventional initial alignment methods, we firstly construct a quaternion-based objective function for stationary SINS using gravity, Earth rate and local latitude information in GD1, and employs gradient descent method to achieve the minimum of the objective function. Secondly, we further improve the quaternion-based objective function in GD2 by using the measurements from IMU to represent the Earth rate instead of using the local latitude directly. Thus, GD2 method is more competent for SINS self-alignment when the local latitude information is not available. In addition, we also analyze the bias errors of accelerometer and gyroscope and the quaternion normality error for GD1 and GD2 method respectively. Moreover, based on the analysis results, a scale factor is also introduced to reduce the alignment errors of GD1 caused by gyroscope biases. Simulation and static experiment are implemented to test the performances of GD1 and GD2 method, and the results verify the accuracy and speed of the proposed methods.

INDEX TERMS SINS self-alignment, gradient descent optimization, stationary base, error analysis.

I. INTRODUCTION

The main task of the self-alignment process of the strapdown inertial navigation system (SINS) is to determine its initial attitude using the measurements of the gravity vector and the Earth rate vector [1]–[3]. As SINS is a dead-reckoning navigation system, an accurate initial attitude determined by the self-alignment process is crucial for guaranteeing the navigation accuracy of SINS [4]–[8]. High accuracy and rapid speed are primary goals for SINS self -alignment. Self-alignment approaches are able to operate using only measurements from internal inertial measurement unit (IMU); without the need for external reference, they are better suited to some applications which require autonomy and/or concealment [9]–[12].

For the restricted problem of aligning on a stationary base, the conventional error model of SINS is not completely observable [13], and the estimability of the states estimated by a Kalman or other optimal estimation-based filter is weak. Poor observability degrades the accuracy and/or speed of the SINS stationary alignment [14]–[16]. We note in passing that multiposition techniques or maneuvering schemes [14], [17]–[19] provide workarounds, but require the base to move, so we do not further consider such schemes.

For a stationary base, the components of the gravity and Earth rate vector in the local geographic navigation frame are constant and can be (pre)computed from local latitude information. The analytical alignment method uses the components of the gravity and Earth rate vector in the navigation frame and their corresponding measurements from IMU to determine the initial attitude [1], [20], [21]. For representing the attitude the most common approaches are Euler angles, direction-cosine matrix (DCM), quaternion and rotating vector [1], [21]–[26]. The DCM-based method

The associate editor coordinating the review of this manuscript and approving it for publication was Rajesh Kumar.

has been widely employed for SINS analytical alignment [1], [21], [26]. In [1], Britting uses three non-coplanar vectors—the gravity vector, the Earth rate vector, and a vector generated by their cross product—to determine the elements of the DCM; consequently, the scheme is called the three-axis attitude determination-based method (TRIAD). Unfortunately, the east alignment error of TRIAD is affected by both the accelerometer and gyroscope biases, with the latter generally dominating the former. The orthogonal-TRIAD (O-TRIAD) method of Jiang [21] instead uses three orthogonal vectors constructed from the cross products of the gravity vector and Earth rate vector to determine the DCM elements, and the resulting east alignment accuracy is improved because it is not affected by gyroscope biases. Additional TRIAD-based methods have been constructed using other choices for the vectors [21], [26], but all have to implement orthogonalization techniques to modify the DCM in order to cope with IMU bias error.

In [25], Li and Fang propose an analytical alignment method and give the explicit expression for attitude represented as Euler angles; for brevity, we refer to this method in this paper as the analytical Euler-angle method (AEA). Silva *et al.* in [9] show that the attitude expression of the AEA method is equivalent to that of the TRIAD method before orthogonalization, and the horizontal component is the same as the O-TRIAD method. Moreover, Silva *et al.* propose an improved O-TRIAD method called orthogonal-normal-TRIAD (ON-TRIAD) in [9] and [27], which also employs the Euler angle to represent the attitude. Additionally, ON-TRIAD can complete the stationary alignment without using the local latitude information. Because there are no orthogonality or normality issues in the Euler angles, the error models of AEA and ON-TRIAD are easier to derive by perturbation methods. In practice, however, because the orthogonality and normality procedures in O-TRIAD may decrease the alignment errors caused by IMU bias, the alignment accuracy of AEA and ON-TRIAD will be inferior to O-TRIAD in many cases.

In this paper we focus on the quaternion representation. Compared with the nine-element DCM, the quaternion vector has only four elements, and hence we need not construct an additional cross product vector to determine the quaternion representation [28]. Additionally, quaternion doesn't have the singularity problem existing in the Euler angle method. Thus, the quaternion is a promising way to represent the attitude. Wu *et al.* in [29] construct the quaternion-based objective function and propose the optimization-based alignment (OBA) method to solve the in-motion alignment problem. As the alignment errors of OBA accumulate with the run-time, it will degrade the alignment accuracy of stationary SINS self-alignment. To deal with stationary SINS self-alignment, the highlight of this paper is that we construct two quaternion-based objective functions on the stationary base and formulate the self-alignment problem as an optimization problem. Moreover, two gradient descent (GD) [30] optimization-based self-alignment methods are proposed to determine the initial attitude in real time.

The first method ("GD1") utilizes the gravity and Earth rate vector in the navigation frame and their corresponding measurements from IMU to construct a quaternion-based objective function. Then GD optimization is employed to achieve the minimum of the objective function. Because the GD1 method still requires the local latitude to be priori known, furthermore, an improved self-alignment method is proposed to solve the self-alignment problem without using local latitude information. Instead, the second method ("GD2") directly uses the measurements from the IMU to represent the components of the Earth rate in the navigation frame, and then constructs an improved quaternion-based objective function. Thus the GD2 method is more competent for SINS initial alignment when the local latitude information is not available. In addition, the error analysis is a challenging but important procedure to evaluate the accuracy of the initial alignment method. We analyze the bias errors of accelerometer and gyroscope and the quaternion normality error for GD1 and GD2 respectively. As the error analysis of the optimization-based method is a quite difficult job, we can only analyze the error models of both methods separately in different ways. Based on the analysis results, a scale factor is also introduced to decrease the attitude error of GD1 caused by gyroscope biases. Furthermore, simulation and static experiment are implemented to test the performances of the proposed methods.

II. GRADIENT DESCENT OPTIMIZATION-BASED SINS SELF-ALIGNMENT METHOD

A. QUATERNION REPRESENTATION

In this paper, we use the East-North-Up (ENU) geographic coordinate system as the navigation frame, and employ the unit quaternion vector to represent the attitude. The quaternion $\boldsymbol{q}_b^n$ represents the transformation from the body frame (subscript or superscript b) to the navigation frame (subscript or superscript n). If $\boldsymbol{q}_b^n = [\,q_0 \quad q_1 \quad q_2 \quad q_3\,]^T$, then the Euler angles ρ (pitch), θ (roll) and ψ (yaw) representation of $\boldsymbol{q}_b^n$ can be expressed as [31]

$$\begin{aligned}\rho &= \mathrm{Asin}(2q_0q_1 + 2q_2q_3)\\ \theta &= \mathrm{Atan2}(2q_0q_2 - 2q_1q_3, 1 - 2q_1^2 - 2q_2^2)\\ \psi &= \mathrm{Atan2}(2q_0q_3 - 2q_1q_2, 1 - 2q_1^2 - 2q_3^2).\end{aligned} \tag{1}$$

where the Euler angles ρ, θ and ψ are determined by the Z-Y-X rotation sequence starting from the navigation frame.

Besides, the transformation between a vector in the navigation frame ($\boldsymbol{r}^n$) and that in the body frame ($\boldsymbol{r}^b$) can be described by

$$\boldsymbol{r}^b = \boldsymbol{q}_n^b \otimes \boldsymbol{r}^n \otimes \boldsymbol{q}_n^{b^*} = \boldsymbol{q}_b^{n^*} \otimes \boldsymbol{r}^n \otimes \boldsymbol{q}_b^n \tag{2}$$

where $\otimes$ denotes the quaternion product, $\boldsymbol{q}_b^{n^*}$ denotes the conjugate quaternion of $\boldsymbol{q}_b^n$ and $\|\boldsymbol{q}_b^n\| = 1$.

B. GRADIENT DESCENT OPTIMIZATION METHOD

In the paper, we formulate SINS self-alignment on the stationary base as an optimization problem, thus the initial attitude can be determined when we achieve the minimum of the objective function. Among these optimization methods for practical applications, the gradient descent method is one of the simplest to both implement and compute [32]. Therefore, we employ gradient descent to determine the four elements of the quaternion vector.

Given $\boldsymbol{r}^n$ and $\boldsymbol{r}^b$, we can construct a suitable objective function to estimate $\boldsymbol{q}_b^n$ using (2)

$$\min_{\boldsymbol{q}_b^n} \boldsymbol{\zeta}(\boldsymbol{q}_b^n, \boldsymbol{r}^n, \widetilde{\boldsymbol{r}}^b) = \frac{1}{2}\left\|\boldsymbol{f}(\boldsymbol{q}_b^n, \boldsymbol{r}^n, \widetilde{\boldsymbol{r}}^b)\right\|^2 \tag{3}$$

$$\begin{aligned}\boldsymbol{f}(\boldsymbol{q}_b^n, \boldsymbol{r}^n, \widetilde{\boldsymbol{r}}^b) &= \boldsymbol{r}^b - \widetilde{\boldsymbol{r}}^b \\ &= \boldsymbol{q}_b^{n^*} \otimes \boldsymbol{r}^n \otimes \boldsymbol{q}_b^n - \widetilde{\boldsymbol{r}}^b\end{aligned} \tag{4}$$

where $\widetilde{\boldsymbol{r}}^b$ is the measurement of $\boldsymbol{r}^b$, $\|\cdot\|$ is Euclidean 2-norm, and the objective function $\boldsymbol{\zeta}(\boldsymbol{q}_b^n, \boldsymbol{r}^n, \widetilde{\boldsymbol{r}}^b)$ is a convex function. It is stressed that the quaternion should be normalized to guarantee $\|\boldsymbol{q}_b^n\| = 1$ during each iteration.

Utilizing gradient descent to solve the objective function in (3) yields

$$\boldsymbol{q}_b^n(k+1) = \boldsymbol{q}_b^n(k) - \lambda \frac{\nabla \boldsymbol{\zeta}(\boldsymbol{q}_b^n, \boldsymbol{r}^n, \widetilde{\boldsymbol{r}}^b)}{\|\nabla \boldsymbol{\zeta}(\boldsymbol{q}_b^n, \boldsymbol{r}^n, \widetilde{\boldsymbol{r}}^b)\|} \tag{5}$$

$$\nabla \boldsymbol{\zeta}(\boldsymbol{q}_b^n, \boldsymbol{r}^n, \widetilde{\boldsymbol{r}}^b) = \boldsymbol{J}^T(\boldsymbol{q}_b^n)\boldsymbol{f}(\boldsymbol{q}_b^n, \boldsymbol{r}^n, \widetilde{\boldsymbol{r}}^b) \tag{6}$$

where λ is a variable step-size, and the Jacobian matrix is

$$\boldsymbol{J}(\boldsymbol{q}_b^n) = \frac{\partial \boldsymbol{f}(\boldsymbol{q}_b^n, \boldsymbol{r}^n, \widetilde{\boldsymbol{r}}^b)}{\partial (\boldsymbol{q}_b^n)^T}.$$

C. SINS SELF-ALIGNMENT METHOD WITH KNOWN LOCAL LATITUDE (GD1)

In this subsection, we focus on the SINS self-alignment for the case where the local latitude information is known. From (3) and (4), we need to construct an objective function whose unique solution determines the quaternion. Because the quaternion contains four elements, a necessary condition for uniqueness is that the objective function has at least four independent constraints. We utilize the gravity vector and Earth rate vector in the navigation frame (the latter computed from the known latitude as shown below) and their measurements from the IMU to construct an objective function.

Firstly, the gravity vector and its normalized form in the navigation frame, as shown in Fig.1, can be written as

$$\boldsymbol{g}^n = \begin{bmatrix} 0 & 0 & 0 & -g \end{bmatrix}^T \tag{7}$$

$$\bar{\boldsymbol{g}}^n = \boldsymbol{g}^n / \|\boldsymbol{g}^n\| = \begin{bmatrix} 0 & 0 & 0 & -1 \end{bmatrix}^T \tag{8}$$

where $\|\boldsymbol{g}^n\| = g$, and g is the magnitude of the gravity vector. Based on (2), the normalized gravity vector in the body frame

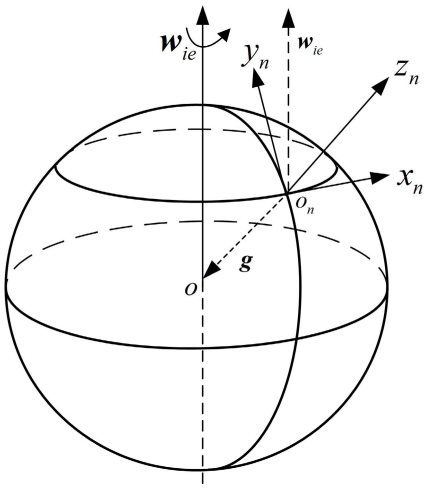

FIGURE 1. The gravity and Earth rate vector in ENU navigation frame.

is expressed as

$$\begin{aligned}\bar{\boldsymbol{g}}^b &= \boldsymbol{q}_n^b \otimes \bar{\boldsymbol{g}}^n \otimes \boldsymbol{q}_n^{b^*} \\ &= \boldsymbol{q}_b^{n^*} \otimes \bar{\boldsymbol{g}}^n \otimes \boldsymbol{q}_b^n\end{aligned} \tag{9}$$

$$\bar{\boldsymbol{g}}^b = \begin{pmatrix} 2(q_0q_2 - q_1q_3) \\ -2(q_0q_1 + q_2q_3) \\ 2q_1^2 + 2q_2^2 - 1 \end{pmatrix} \tag{10}$$

We also define the gravity vector measurement (by three-axis accelerometer) in the body frame

$$\widetilde{\bar{\boldsymbol{g}}}^b = \begin{bmatrix} \widetilde{g}_x^b & \widetilde{g}_y^b & \widetilde{g}_z^b \end{bmatrix}^T \tag{11}$$

Secondly, the Earth rate, as shown in Fig.1, and its normalized form in the navigation frame can be represented as

$$\boldsymbol{w}^n = \begin{bmatrix} 0 & 0 & w_{ie}\cos L & w_{ie}\sin L \end{bmatrix}^T \tag{12}$$

$$\bar{\boldsymbol{w}}^n = \boldsymbol{w}^n / \|\boldsymbol{w}^n\| = \begin{bmatrix} 0 & 0 & \cos L & \sin L \end{bmatrix}^T \tag{13}$$

where $\|\boldsymbol{w}^n\| = w_{ie}$, w_{ie} denotes the magnitude of the Earth rate and L denotes the local latitude (which is assumed to be priori known for this method). We can then write the normalized Earth rate vector in the body frame as

$$\bar{\boldsymbol{w}}^b = \boldsymbol{q}_b^{n^*} \otimes \bar{\boldsymbol{w}}^n \otimes \boldsymbol{q}_b^n \tag{14}$$

$$\bar{\boldsymbol{w}}^b = \begin{pmatrix} 2(q_1q_2 + q_0q_3)\cos L + 2(q_1q_3 - q_0q_2)\sin L \\ (1 - 2q_1^2 - 2q_3^2)\cos L + 2(q_0q_1 + q_2q_3)\sin L \\ 2(q_2q_3 - q_0q_1)\cos L + (1 - 2q_1^2 - 2q_2^2)\sin L \end{pmatrix} \tag{15}$$

Finally, we define the Earth rate vector measurement (by three-axis gyroscope) in the body frame

$$\widetilde{\bar{\boldsymbol{w}}}^b = \begin{bmatrix} \widetilde{w}_x^b & \widetilde{w}_y^b & \widetilde{w}_z^b \end{bmatrix}^T \tag{16}$$

As the measurements of the gravity vector or the Earth rate vector alone cannot provide a unique solution to determine

the quaternion from (4), we combine both of them to construct a united function

$$\begin{aligned}
&\boldsymbol{f}(\boldsymbol{q}_b^n, \boldsymbol{g}, \boldsymbol{w}) \\
&= \begin{pmatrix} \boldsymbol{f}_g(\boldsymbol{q}_b^n, \boldsymbol{g}) \\ \boldsymbol{f}_w(\boldsymbol{q}_b^n, \boldsymbol{w}) \end{pmatrix} = \begin{pmatrix} \bar{\boldsymbol{g}}^b - \widetilde{\boldsymbol{g}}^b/g \\ \bar{\boldsymbol{w}}^b - \widetilde{\boldsymbol{w}}^b/w_{ie} \end{pmatrix} \\
&= \begin{pmatrix} 2(q_0q_2 - q_1q_3) - \widetilde{g}_x^b/g \\ -2(q_0q_1 + q_2q_3) - \widetilde{g}_y^b/g \\ (2q_1^2 + 2q_2^2 - 1) - \widetilde{g}_z^b/g \\ 2(q_1q_2 + q_0q_3)\cos L + 2(q_1q_3 - q_0q_2)\sin L - \widetilde{w}_x^b/w_{ie} \\ (1 - 2q_1^2 - 2q_3^2)\cos L + 2(q_0q_1 + q_2q_3)\sin L - \widetilde{w}_y^b/w_{ie} \\ 2(q_2q_3 - q_0q_1)\cos L + (1 - 2q_1^2 - 2q_2^2)\sin L - \widetilde{w}_z^b/w_{ie} \end{pmatrix}
\end{aligned} \tag{17}$$

whose Jacobian is

$$\boldsymbol{J}(\boldsymbol{q}_b^n) = \frac{\partial \boldsymbol{f}(\boldsymbol{q}_b^n, \boldsymbol{g}, \boldsymbol{w})}{\partial (\boldsymbol{q}_b^n)^T} = \begin{pmatrix} \dfrac{\partial \boldsymbol{f}_g(\boldsymbol{q}_b^n, \boldsymbol{g})}{\partial (\boldsymbol{q}_b^n)^T} \\ \dfrac{\partial \boldsymbol{f}_w(\boldsymbol{q}_b^n, \boldsymbol{w})}{\partial (\boldsymbol{q}_b^n)^T} \end{pmatrix} \tag{18}$$

where

$$\frac{\partial \boldsymbol{f}_g(\boldsymbol{q}_b^n, \boldsymbol{g})}{\partial (\boldsymbol{q}_b^n)^T} = \begin{pmatrix} 2q_2 & -2q_3 & 2q_0 & -2q_1 \\ -2q_1 & -2q_0 & -2q_3 & -2q_2 \\ 0 & 4q_1 & 4q_2 & 0 \end{pmatrix} \tag{19}$$

and

$$\begin{aligned}
&\frac{\partial \boldsymbol{f}_w(\boldsymbol{q}_b^n, \boldsymbol{w})}{\partial (\boldsymbol{q}_b^n)^T} \\
&= \begin{pmatrix} 2q_3\cos L - 2q_2\sin L & 2q_2\cos L + 2q_3\sin L \\ 2q_1\sin L & -4q_1\cos L + 2q_0\sin L \\ -2q_1\cos L & -2q_0\cos L - 4q_1\sin L \\ 2q_1\cos L - 2q_0\sin L & 2q_0\cos L + 2q_1\sin L \\ 2q_3\sin L & -4q_3\cos L + 2q_2\sin L \\ 2q_3\cos L - 4q_2\sin L & 2q_2\cos L \end{pmatrix}
\end{aligned} \tag{20}$$

With these definitions, the quaternion vector can be determined by minimizing the objective function $\boldsymbol{\zeta}(\boldsymbol{q}_b^n, \boldsymbol{g}, \boldsymbol{w})$ with a gradient descent optimization algorithm. In this case (3) and (4) take the form

$$\boldsymbol{q}_b^n(k+1) = \boldsymbol{q}_b^n(k) - \lambda_k \frac{\nabla \boldsymbol{\zeta}(\boldsymbol{q}_b^n, \boldsymbol{g}, \boldsymbol{w})}{\|\nabla \boldsymbol{\zeta}(\boldsymbol{q}_b^n, \boldsymbol{g}, \boldsymbol{w})\|} \tag{21}$$

$$\nabla \boldsymbol{\zeta}(\boldsymbol{q}_b^n, \boldsymbol{g}, \boldsymbol{w}) = \boldsymbol{J}^T(\boldsymbol{q}_b^n) \boldsymbol{f}(\boldsymbol{q}_b^n, \boldsymbol{g}, \boldsymbol{w}) \tag{22}$$

Due to the existence of bias errors in the accelerometer and gyroscope, we must normalize the quaternion at each iteration. In addition, the iteration step size λ_k in (21) is a function of the sampling time or iteration time. Based on [32], we calculate λ_k as

$$\lambda_k = \beta_k \Delta t \tag{23}$$

where β_k is a scale factor related to physical measurement dynamics and Δt is the sampling period. We observe that an appropriate choice of the iteration step-size λ_k, or equivalently the scale factor β_k, is crucial to improve the convergence rate. Generally, both convergence rate and accuracy highly depend on the choice of β [30], [33]. The convergence rate will be faster with a large β, but such a choice may degrade the algorithm's accuracy. On the other hand, we can achieve a more accurate result with a small β, but the iteration will take longer to converge to this result. We recommend to choose a time-varying β that declines gradually with iteration step for the SINS self-alignment application. We will also mention in passing that the convergence rate of gradient descent optimization can be accelerated through advanced gradient descent optimizers, such as the Momentum, Adagrad and Adam algorithms [34]; however, we will not discuss these accelerations further here.

D. SINS SELF-ALIGNMENT METHOD WITH NO LOCAL LATITUDE (GD2)

In last subsection, we notice that the proposed self-alignment method (GD1) cannot be implemented unless we obtain the local latitude in advance. In fact, most existing SINS alignment methods, to the best of our knowledge, all require that the local latitude information has to be known in advance. The local latitude information, however, may be inaccurate or hard to obtain in some situations, such as the electronic interferences and GPS outages. Under these situations, the conventional self-methods will fail to determine the initial attitude. To deal with the SINS self-alignment problem with no local latitude information, we propose an improvement on the gradient descent optimization-based SINS self-alignment method (GD2) in this subsection.

From (13), it is noted that there are only y-axis and z-axis components of the Earth rate vector in the navigation frame. Thus, the general form of the normalized Earth rate vector in the navigation frame can be represented by (24).

$$\bar{\boldsymbol{w}}^n = \begin{bmatrix} 0 & 0 & \bar{w}_y & \bar{w}_z \end{bmatrix}^T \tag{24}$$

On the other hand, based on (1), (10) and (17), the horizontal attitude (pitch ρ and roll θ) can be determined directly from the outputs of three-axis accelerometer. The pitch ρ and roll θ can be rewritten as

$$\begin{aligned}
\rho &= -\mathrm{Asin}(\widetilde{g}_y^b/g) \\
\theta &= -\mathrm{Atan2}(\widetilde{g}_x^b, \widetilde{g}_z^b)
\end{aligned} \tag{25}$$

Therefore, by using only the accelerometer measurements, we can determine an orthogonal coordinate frame, of which the horizontal plane is aligned with that of the navigation frame. We set the initial yaw in the new orthogonal frame as 0°, so the deviation angle between the new orthogonal frame and the navigation frame is the yaw angle, as denoted by Fig.2. Besides, the transformation of the Earth rate vector measured by the three-axis gyroscope from body frame to the new orthogonal frame is described by (26) and (27).

$$\widehat{\boldsymbol{w}}^n = \boldsymbol{q}_b^n \otimes \frac{\widetilde{\boldsymbol{w}}^b}{w_{ie}} \otimes \boldsymbol{q}_b^{n^*} \tag{26}$$

$$\widehat{\boldsymbol{w}}^n = \begin{bmatrix} 0 & \widehat{w}_x & \widehat{w}_y & \widehat{w}_z \end{bmatrix}^T \tag{27}$$

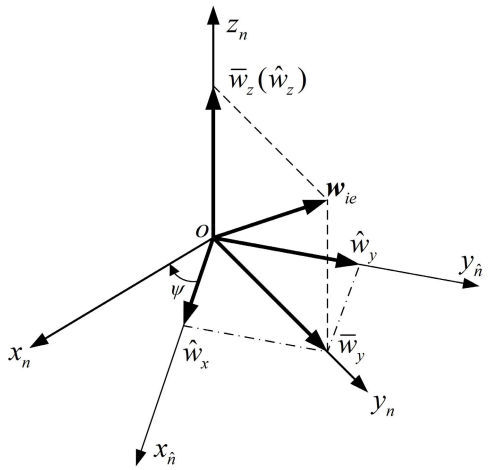

FIGURE 2. The projection of Earth rate vector in navigation frame and new orthogonal frame.

Furthermore, the projection of the Earth rate vector on the horizontal plane of the new orthogonal frame equals to its y-axis component in the navigation frame ($\bar{w}_y$), as illustrated by Fig.2, and the z-axis component of the Earth rate vector in the new orthogonal frame equals to its z-axis component in the navigation frame ($\bar{w}_z$). Thus we can obtain (28).

$$\begin{cases} \bar{w}_y = \sqrt{\widehat{w}_x^2 + \widehat{w}_y^2} \\ \bar{w}_z = \widehat{w}_z \end{cases} \tag{28}$$

And then, the normalized Earth rate vector $\bar{\boldsymbol{w}}^n$ in (13) can be estimated as

$$\bar{\boldsymbol{w}}^n = \begin{bmatrix} 0 & 0 & \sqrt{\widehat{w}_x^2 + \widehat{w}_y^2} & \widehat{w}_z \end{bmatrix}^T \tag{29}$$

At this point, the Earth rate vector in the navigation frame ($\bar{\boldsymbol{w}}^n$) is obtained by using the measurements from the IMU instead of directly using local latitude information. Then substituting (29) into (14) yields the corresponding Earth rate vector in the body frame ($\bar{\boldsymbol{w}}^b$).

$$\bar{\boldsymbol{w}}^b = \begin{pmatrix} 2(q_1q_2 + q_0q_3)\sqrt{\widehat{w}_x^2 + \widehat{w}_y^2} + 2(q_1q_3 - q_0q_2)\widehat{w}_z \\ (1 - 2q_1^2 + 2q_3^2)\sqrt{\widehat{w}_x^2 + \widehat{w}_y^2} + 2(q_0q_1 + q_2q_3)\widehat{w}_z \\ 2(q_2q_3 - q_0q_1)\sqrt{\widehat{w}_x^2 + \widehat{w}_y^2} + (1 - 2q_1^2 - 2q_2^2)\widehat{w}_z \end{pmatrix} \tag{30}$$

Hence, $\boldsymbol{f}_w(\boldsymbol{q}_b^n, \boldsymbol{w})$ in (17) is renewed as

$$\begin{aligned} &\boldsymbol{f}_w(\boldsymbol{q}_b^n, \boldsymbol{w}) \\ &= \begin{pmatrix} 2(q_1q_2 + q_0q_3)\sqrt{\widehat{w}_x^2 + \widehat{w}_y^2} + 2(q_1q_3 - q_0q_2)\widehat{w}_z - \widetilde{w}_x^b / w_{ie} \\ (1 - 2q_1^2 - 2q_3^2)\sqrt{\widehat{w}_x^2 + \widehat{w}_y^2} + 2(q_0q_1 + q_2q_3)\widehat{w}_z - \widetilde{w}_y^b / w_{ie} \\ 2(q_2q_3 - q_0q_1)\sqrt{\widehat{w}_x^2 + \widehat{w}_y^2} + (1 - 2q_1^2 - 2q_2^2)\widehat{w}_z - \widetilde{w}_z^b / w_{ie} \end{pmatrix} \end{aligned} \tag{31}$$

Substituting (31) into (17) gives a new objective function without using local latitude information. Moreover, utilizing gradient descent optimization algorithm to minimize the new obtained objective function, as represented by (18)-(22), can determine the quaternion vector $\boldsymbol{q}_b^n$.

III. ERROR ANALYSIS

In this section, we will analyze the error models of the proposed SINS self-algorithms in Section II. For convenience, we respectively call these two gradient descent methods as GD1 method (using local latitude) and GD2 method (without using local latitude) in the following. We only consider the influences of accelerometer and gyroscope biases, which are considered as constant values during a fast initial alignment process. More specifically, ∇_g^b and ∇_w^b denote the bias error of accelerometer and gyroscope in $\boldsymbol{f}_g(\boldsymbol{q}_b^n, \boldsymbol{g})$ and $\boldsymbol{f}_w(\boldsymbol{q}_b^n, \boldsymbol{w})$, respectively.

A. GD1 METHOD

According to (17)-(22), the update of $\boldsymbol{f}_g(\boldsymbol{q}_b^n, \boldsymbol{g})$ and $\boldsymbol{f}_w(\boldsymbol{q}_b^n, \boldsymbol{w})$ during each iteration are mutually independent before (21). Thus, consider $\boldsymbol{f}_g(\boldsymbol{q}_b^n, \boldsymbol{g})$ and $\boldsymbol{f}_w(\boldsymbol{q}_b^n, \boldsymbol{w})$ in (17) separately, and let

$$\begin{aligned} \boldsymbol{f}_g(\boldsymbol{q}_0, \boldsymbol{g}) &= \bar{\boldsymbol{g}}^b(\boldsymbol{q}_0) - \boldsymbol{g}^b = \boldsymbol{0} \\ \boldsymbol{f}_g(\boldsymbol{q}_1, \boldsymbol{g}) &= \bar{\boldsymbol{g}}^b(\boldsymbol{q}_1) - \boldsymbol{g}^b - \nabla_g^b = \boldsymbol{0} \\ \boldsymbol{f}_g(\boldsymbol{q}_b^n, \boldsymbol{g}) &= \bar{\boldsymbol{g}}^b(\boldsymbol{q}_b^n) - \boldsymbol{g}^b - \nabla_g^b \end{aligned} \tag{32}$$

where $\boldsymbol{q}_0$ is the ideal quaternion without any errors, and $\boldsymbol{g}^b$ is the corresponding accelerometer measurement; $\boldsymbol{q}_1$ is the quaternion disturbed by accelerometer bias ∇_g^b alone, $\boldsymbol{q}_b^n$ is the actual estimated quaternion disturbed by both accelerometer bias and gyroscope bias, and the additional quaternion error $\delta\boldsymbol{q} = \boldsymbol{q}_b^n - \boldsymbol{q}_0$. Thus, the value of $\boldsymbol{f}_g(\boldsymbol{q}_b^n, \boldsymbol{g})$ or the difference between $\boldsymbol{f}_g(\boldsymbol{q}_b^n, \boldsymbol{g})$ and $\boldsymbol{f}_g(\boldsymbol{q}_1, \boldsymbol{g})$ denotes the error affected by the gyroscope bias.

According to (32), ignoring the second and higher order terms of the differential of $\bar{\boldsymbol{g}}^b(\boldsymbol{q}_0)$, we have

$$\begin{aligned} &\boldsymbol{f}_g(\boldsymbol{q}_b^n, \boldsymbol{g}) - \boldsymbol{f}_g(\boldsymbol{q}_1, \boldsymbol{g}) \\ &= \bar{\boldsymbol{g}}^b(\boldsymbol{q}_b^n) - \bar{\boldsymbol{g}}^b(\boldsymbol{q}_1) \\ &= \bar{\boldsymbol{g}}^b(\boldsymbol{q}_b^n) - \bar{\boldsymbol{g}}^b(\boldsymbol{q}_0) - \nabla_g^b \\ &\approx \frac{\partial \bar{\boldsymbol{g}}^b(\boldsymbol{q}_0)}{\partial (\boldsymbol{q}_0)^T} \delta\boldsymbol{q} - \nabla_g^b \end{aligned} \tag{33}$$

$$\frac{\partial \bar{\boldsymbol{g}}^b(\boldsymbol{q}_0)}{\partial (\boldsymbol{q}_0)^T} \delta\boldsymbol{q} = \boldsymbol{f}_g(\boldsymbol{q}_b^n, \boldsymbol{g}) + \nabla_g^b \tag{34}$$

For $\boldsymbol{f}_w(\boldsymbol{q}_b^n, \boldsymbol{w})$, similarly we obtain

$$\frac{\partial \bar{\boldsymbol{w}}^b(\boldsymbol{q}_0)}{\partial (\boldsymbol{q}_0)^T} \delta\boldsymbol{q} = \boldsymbol{f}_w(\boldsymbol{q}_b^n, \boldsymbol{w}) + \nabla_w^b \tag{35}$$

Combining (34) and (35) yields

$$\begin{pmatrix} \dfrac{\partial \bar{\boldsymbol{g}}^b(\boldsymbol{q}_0)}{\partial (\boldsymbol{q}_0)^T} \\ \dfrac{\partial \bar{\boldsymbol{w}}^b(\boldsymbol{q}_0)}{\partial (\boldsymbol{q}_0)^T} \end{pmatrix} \delta\boldsymbol{q} = \begin{pmatrix} \boldsymbol{f}_g(\boldsymbol{q}_b^n, \boldsymbol{g}) + \nabla_g^b \\ \boldsymbol{f}_w(\boldsymbol{q}_b^n, \boldsymbol{w}) + \nabla_w^b \end{pmatrix} \tag{36}$$

Therefore, the quaternion error $\delta\boldsymbol{q}$ is expressed as

$$\delta\boldsymbol{q} = (\boldsymbol{A}^T\boldsymbol{A})^{-1}\boldsymbol{A}^T\boldsymbol{B} \tag{37}$$

where $\boldsymbol{A} = \begin{pmatrix} \frac{\partial \tilde{\boldsymbol{g}}^b(\boldsymbol{q}_0)}{\partial(\boldsymbol{q}_0)^T} \\ \frac{\partial \tilde{\boldsymbol{w}}^b(\boldsymbol{q}_0)}{\partial(\boldsymbol{q}_0)^T} \end{pmatrix}$, $\boldsymbol{B} = \begin{pmatrix} \boldsymbol{f}_g(\boldsymbol{q}_b^n, \boldsymbol{g}) + \nabla_g^b \\ \boldsymbol{f}_w(\boldsymbol{q}_b^n, \boldsymbol{w}) + \nabla_w^b \end{pmatrix}$, and both $\boldsymbol{A}$ and $\boldsymbol{B}$ are column full rank matrices.

According to (1) and (37), the expression of the attitude error of GD1 method is obtained using the perturbation method, as denoted by (38).

$$\begin{aligned} d\rho &= dq_\rho/\cos(\rho) \\ d\theta &= (dq_{\theta_1}q_{\theta_2} - q_{\theta_1}dq_{\theta_2})/(q_{\theta_1}^2 + q_{\theta_2}^2) \\ d\psi &= (dq_{\psi_1}q_{\psi_2} - q_{\psi_1}dq_{\psi_2})/(q_{\psi_1}^2 + q_{\psi_2}^2) \end{aligned} \tag{38}$$

where $q_\rho = (2q_0q_1 + 2q_2q_3)$, $q_{\theta_1} = 2q_0q_2 - 2q_1q_3$, $q_{\theta_2} = 1 - 2q_1^2 - 2q_2^2$, $q_{\psi_1} = 2q_0q_3 - 2q_1q_2$, $q_{\psi_2} = 1 - 2q_1^2 - 2q_3^2$, and $dq_\rho, dq_{\theta_1}, dq_{\theta_2}, dq_{\psi_1}, dq_{\psi_2}$ are represented by $\delta\boldsymbol{q}$ in (37). (Unfortunately, we cannot give the attitude error expression in the form of sensor errors, or it would be better for demonstrating the influences of sensor errors on the alignment accuracy.)

Moreover, we will introduce a scale factor to decrease the horizontal errors of GD1 method in the following, because we notice that the horizontal attitude errors of GD1 method after quaternion normalization process are affected by both accelerometer and gyroscope biases. Comparing $\boldsymbol{f}_g(\boldsymbol{q}_1, \boldsymbol{g})$ and $\boldsymbol{f}_g(\boldsymbol{q}_b^n, \boldsymbol{g})$ in (32), and considering (33)-(34), we deduce that $\boldsymbol{f}_g(\boldsymbol{q}_b^n, \boldsymbol{g})$ is the error affected by ∇_w^b. Similarly, $\boldsymbol{f}_w(\boldsymbol{q}_b^n, \boldsymbol{w})$ is the error affected by ∇_g^b. In fact, both $\boldsymbol{f}_g(\boldsymbol{q}_b^n, \boldsymbol{g})$ and $\boldsymbol{f}_w(\boldsymbol{q}_b^n, \boldsymbol{w})$ are the errors mainly caused by the quaternion normalization. In order to diminish the horizontal errors or $\delta\boldsymbol{q}$, we need to decrease $\boldsymbol{f}_g(\boldsymbol{q}_b^n, \boldsymbol{g})$ or/and $\boldsymbol{f}_w(\boldsymbol{q}_b^n, \boldsymbol{w})$ in (37) since $\boldsymbol{A}$, ∇_g^b and ∇_w^b are fixed values.

According to (17)-(18), (22) can be rewritten as

$$\begin{aligned} \nabla\boldsymbol{\zeta}(\boldsymbol{q}_b^n, \boldsymbol{g}, \boldsymbol{w}) &= \boldsymbol{J}_g^T(\boldsymbol{q}_b^n)\boldsymbol{f}_g(\boldsymbol{q}_b^n, \boldsymbol{g}) + \boldsymbol{J}_w^T(\boldsymbol{q}_b^n)\boldsymbol{f}_w(\boldsymbol{q}_b^n, \boldsymbol{w}) \\ &= \nabla\boldsymbol{\zeta}_g + \nabla\boldsymbol{\zeta}_w \\ &= \dot{\boldsymbol{q}} + \delta\dot{\boldsymbol{q}}_g + \delta\dot{\boldsymbol{q}}_w \end{aligned} \tag{39}$$

where $J_g(\boldsymbol{q}_b^n) = \frac{\partial \boldsymbol{f}_g(\boldsymbol{q}_b^n, \boldsymbol{g})}{\partial(\boldsymbol{q}_b^n)^T}$, $J_w(\boldsymbol{q}_b^n) = \frac{\partial \boldsymbol{f}_w(\boldsymbol{q}_b^n, \boldsymbol{w})}{\partial(\boldsymbol{q}_b^n)^T}$; $\delta\dot{\boldsymbol{q}}_g$ and $\delta\dot{\boldsymbol{q}}_w$ are the errors affected by ∇_g^b and ∇_w^b, and $\dot{\boldsymbol{q}}$ is the quaternion rate without being affected by ∇_g^b and ∇_w^b during an iteration.

In practice, the bias error influence of ∇_w^b on alignment result generally is larger than that of ∇_g^b, hence we introduce a scale factor α to decrease the weight of $\delta\dot{\boldsymbol{q}}_w$ in (39). Furthermore, (39) is rewritten as

$$\begin{aligned} &\nabla\boldsymbol{\zeta}(\boldsymbol{q}_b^n, \boldsymbol{g}, \boldsymbol{w}) \\ &= \dot{\boldsymbol{q}} + \alpha\delta\dot{\boldsymbol{q}}_g + (1-\alpha)\delta\dot{\boldsymbol{q}}_w \\ &= \alpha\nabla\boldsymbol{\zeta}_g + (1-\alpha)\nabla\boldsymbol{\zeta}_w \\ &= \alpha\boldsymbol{J}_g^T(\boldsymbol{q}_b^n)\boldsymbol{f}_g(\boldsymbol{q}_b^n, \boldsymbol{g}) + (1-\alpha)\boldsymbol{J}_w^T(\boldsymbol{q}_b^n)\boldsymbol{f}_w(\boldsymbol{q}_b^n, \boldsymbol{w}) \end{aligned} \tag{40}$$

where α can be set as $0.5 \le \alpha < 1$.

Therefore, a quaternion vector with better accuracy can be achieved by substituting (40) into (21) for the gradient descent optimization.

B. GD2 METHOD

Though the gradient descent optimization for GD1 and GD2 method are similar to each other, the error models of them are different. In GD2 method, we use the outputs of accelerometers and gyroscopes to represent the Earth rate vector in navigation frame ($\bar{\boldsymbol{w}}^n$) in (29), which is corrupted by the accelerometer and gyroscope biases. Consequently, we cannot analyze the error model of GD2 method using the way for GD1, as we cannot derive the expression of $\boldsymbol{f}_w(\boldsymbol{q}_b^n, \boldsymbol{w})$ as represented by (35).

Instead, the basic idea of GD2 method is firstly utilizing the accelerometer outputs to determine the horizontal attitude, and then determining the yaw angle with the outputs of accelerometers and gyroscopes, which is the same as the Analytical Euler-Angle (AEA) method. On the other hand, as the objective function of GD2 is a standard convex function, its optimal solution for minimizing the objective function is unique. That is, it will be the unique solution if it yields the minimum result. Therefore, based on (25) and the conclusion of AEA method in [25], we give the explicit attitude expression of GD2 method in terms of Euler angle without derivations in (41), and numerical results in Appendix illustrate that (41) is an optimal solution to yield the minimum result.

$$\begin{aligned} \rho &= \mathrm{Asin}(-\tilde{g}_y^b/\tilde{g}) \\ \theta &= \mathrm{Atan2}(-\tilde{g}_x^b, \tilde{g}_z^b) \\ \psi &= \mathrm{Atan2}(\tilde{g}_x^b\tilde{w}_z^b - \tilde{g}_z^b\tilde{w}_x^b, \tilde{g}\tilde{w}_y^b + \tilde{f}_y^b\bar{w}_z) \end{aligned} \tag{41}$$

where $\tilde{g}$ is the magnitude of gravity vector measured by accelerometer, $\tilde{g} = \mathrm{norm}(\tilde{g}_x^b, \tilde{g}_y^b, \tilde{g}_z^b)$; $\bar{w}_z$ is z-axis component of the estimated Earth rate in navigation frame ($\bar{\boldsymbol{w}}^n$), and $\bar{w}_z = \widehat{w}_z = -\sin(\theta)\cos(\rho)\tilde{w}_x^b + \sin(\rho)\tilde{w}_y^b + \cos(\theta)\cos(\rho)\tilde{w}_z^b$

Apart from analyzing the influence of bias errors, we also analyze the quaternion normality error of GD2 method. Hence, the perturbation method is employed to analyze the influences of bias errors and normality errors, and the attitude errors are given, up to one order of time, by

$$\begin{aligned} d\rho &= \frac{\partial\rho}{\partial\tilde{g}_y^b}d\tilde{g}_y^b + \frac{\partial\rho}{\partial\tilde{g}}d\tilde{g} \\ &= -\frac{1}{\cos(\rho)}\left(\frac{d\tilde{g}_y^b}{\tilde{g}} - \frac{\tilde{g}_y^b d\tilde{g}}{\tilde{g}^2}\right) \\ &\approx -\frac{\nabla_{gy}^b}{g\cos(\rho)} - \frac{d\tilde{g}}{g}\tan(\rho) \end{aligned} \tag{42}$$

$$\begin{aligned} d\theta &= \frac{\partial\theta}{\partial\tilde{g}_x^b}d\tilde{g}_x^b + \frac{\partial\theta}{\partial\tilde{g}_z^b}d\tilde{g}_z^b \\ &= -\frac{1}{1+\tan^2(\theta)}\left(\frac{d\tilde{g}_x^b}{\tilde{g}_z^b} - \frac{\tilde{g}_x^b d\tilde{g}_z^b}{(\tilde{g}_z^b)^2}\right) \\ &\approx \frac{\sin(\theta)\nabla_{gz}^b + \cos(\theta)\nabla_{gx}^b}{g\cos(\rho)} \end{aligned} \tag{43}$$

where $d\bar{w}_z$ is the estimate errors of z-axis component of the Earth rate ($\bar{w}_z$), which is mainly caused by accelerometer and gyroscope biases; $d\widetilde{g} = \widetilde{g} - g = \sin(\theta)\cos(\rho)\nabla^b_{gx} - \sin(\rho)\nabla^b_{gy} - \cos(\theta)\cos(\rho)\nabla^b_{gz}$, and the term with $d\widetilde{g}$ in (42) and (43) are the normality errors caused by quaternion normalization. Particularly, for (42), supposing that $|\rho| \leq 45°$, $|\theta| \leq 45°$ and $\nabla^b_{gx} = \nabla^b_{gy} = \nabla^b_{gz}$, then $-1.5\nabla^b_{gy} < d\widetilde{g}\sin(\rho) \leq 0.5\nabla^b_{gy}$. Hence, the normality error term $\frac{d\widetilde{g}}{g}\tan(\rho)$ in (42) cannot be ignored in some applications.

IV. SIMULATION AND EXPERIMENT RESULTS

To verify the performances of the proposed gradient descent optimization-based SINS self-alignment methods, simulation and static experiment are carried out in this section. Besides, several popular SINS self-alignment methods—O-TRIAD [21], ON-TRIAD [9] and AEA [25] and optimization-based alignment (OBA) [29] are employed for comparisons.

A. SIMULATION RESULTS

In this section, several simulations are implemented to test the performance of the proposed GD1 and GD2 methods under the stationary base. For the convenience of error analysis, we mainly investigate the influences of accelerometer and gyroscope constant biases, ∇^b_g and ∇^b_w, in the simulation. Particularly, $\nabla^b_{gi} = 100\mu g$ and $\nabla^b_{wi} = 0.01°/h$, $i = x, y, z$. Besides, the local latitude is 45.7796° and the sampling rate is 100 Hz.

First of all, simulation is implemented to test the dynamic characteristics and alignment errors of GD1 and GD2 method seprately, and three initial attitudes (10°, 10°, 45°), (10°, 10°, 90°), (10°, 10°, 135°), are selected to demonstrate the performances of GD1 and GD2. In order to guarantee that the gradient descent optimization method comes to converge, it is set to take 2000 iterations for each initial attitude.

Figs. 3-4 and Table 1 describe the dynamic convergence characteristics and estimate errors of GD1 and GD2 for different initial attitudes, respectively. It is noted that the horizontal attitude errors of GD1 ($d\rho$ and $d\theta$) differ in the yaw angle. As demonstrated by Figs. 3-4, both GD1 and GD2 take more iterations to converge for the larger initial yaw angle. Table 1 shows that GD1 and GD2 take about 8 ms for each 2000-iteration optimization, which is the average cost time of 400 sample points in the simulation, and it also

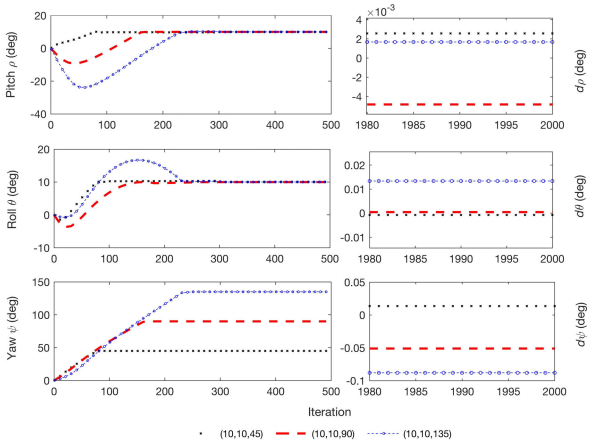

FIGURE 3. Dynamic characteristics and alignment errors of GD1.

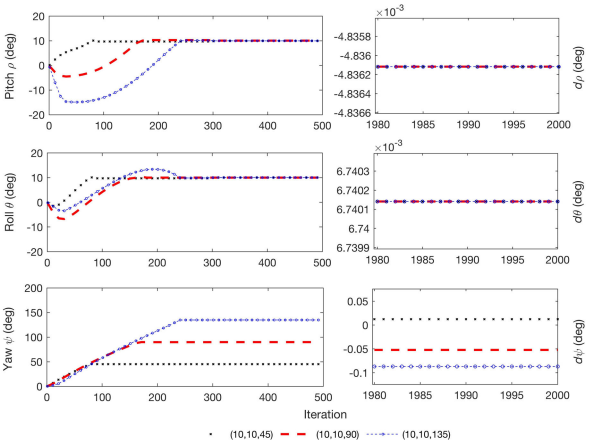

FIGURE 4. Dynamic characteristics and alignment errors of GD2.

indicates that GD1 and GD2 are capable for the real-time applications.

Secondly, simulation is performed to investigate the error characteristics of GD1 and GD2 with different yaw angles. In the simulation, the yaw angle varies from 0° ∼ 360° with fixed pitch and roll angle (10°, 10°). Besides, a series of scale factor α are selected to verify the performance of the method in (40) on improving alignment accuracy of GD1 method.

Fig.5 describes the error characteristics of GD1 and GD2 methods when yaw angle varying from 0° ∼ 360°. Specifically, Fig.5(a) denotes the alignment error of

$$
\begin{aligned}
d\psi &= \frac{\partial\psi}{\partial\widetilde{g}^b_x}d\widetilde{g}^b_x + \frac{\partial\psi}{\partial\widetilde{w}^b_z}d\widetilde{w}^b_z + \frac{\partial\psi}{\partial\widetilde{g}^b_z}d\widetilde{g}^b_z + \frac{\partial\psi}{\partial\widetilde{w}^b_x}d\widetilde{w}^b_x + \frac{\partial\psi}{\partial\widetilde{w}^b_y}d\widetilde{w}^b_y + \frac{\partial\psi}{\partial\widetilde{g}^b_y}d\widetilde{g}^b_y + \frac{\partial\psi}{\partial\widetilde{g}}d\widetilde{g} + \frac{\partial\psi}{\partial\bar{w}_z}d\bar{w}_z \\
&= \frac{1}{1+\tan^2(\psi)}\left(\frac{d(\widetilde{g}^b_x\widetilde{w}^b_z - \widetilde{g}^b_z\widetilde{w}^b_x)}{\widetilde{g}\widetilde{w}^b_y + \widetilde{f}^b_y\bar{w}_z} - \frac{(\widetilde{g}^b_x\widetilde{w}^b_z - \widetilde{g}^b_z\widetilde{w}^b_x)d(\widetilde{g}\widetilde{w}^b_y + \widetilde{f}^b_y\bar{w}_z)}{(\widetilde{g}\widetilde{w}^b_y + \widetilde{f}^b_y\bar{w}_z)^2}\right) \\
&\approx \frac{(\nabla^b_{gx}\widetilde{w}^b_z + \widetilde{g}^b_x\nabla^b_{wz} - \nabla^b_{gz}\widetilde{w}^b_x - \widetilde{g}^b_z\nabla^b_{wx})(\widetilde{g}\widetilde{w}^b_y + \widetilde{f}^b_y\bar{w}_z)}{(\widetilde{g}^b_x\widetilde{w}^b_z - \widetilde{g}^b_z\widetilde{w}^b_x)^2 + (\widetilde{g}\widetilde{w}^b_y + \widetilde{f}^b_y\bar{w}_z)^2} - \frac{(\widetilde{g}^b_x\widetilde{w}^b_z - \widetilde{g}^b_z\widetilde{w}^b_x)(d\widetilde{g}\,\widetilde{w}^b_y + \widetilde{g}\,\nabla^b_{wy} + \nabla^b_{gy}\bar{w}_z + \widetilde{f}^b_y d\bar{w}_z)}{(\widetilde{g}^b_x\widetilde{w}^b_z - \widetilde{g}^b_z\widetilde{w}^b_x)^2 + (\widetilde{g}\widetilde{w}^b_y + \widetilde{f}^b_y\bar{w}_z)^2}
\end{aligned}
\tag{44}
$$

TABLE 1. Alignment errors and cost time of GD1 and GD2.

Methods	$d\rho$ (deg)	$d\theta$ (deg)	$d\psi$ (deg)			Time(ms)
	10	10	45	90	135	
GD1	$2.56e^{-3}$	$-7.76e^{-4}$	$1.36e^{-2}$	—	—	8.10
	$-4.83e^{-3}$	$4.23e^{-4}$	—	$-5.11e^{-2}$	—	8.06
	$1.68e^{-3}$	$1.34e^{-2}$	—	—	$-8.80e^{-2}$	8.14
GD2	$-4.84e^{-3}$	$6.74e^{-3}$	$1.23e^{-2}$	—	—	8.13
	$-4.84e^{-3}$	$6.74e^{-3}$	—	$-5.22e^{-2}$	—	8.14
	$-4.84e^{-3}$	$6.74e^{-3}$	—	—	$-8.68e^{-2}$	8.02

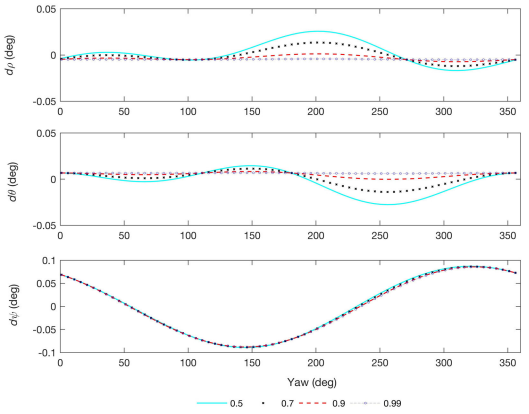

(a)

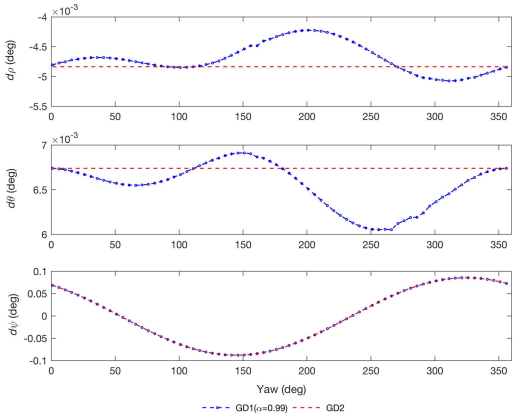

(b)

FIGURE 5. Alignment error comparisons of GD1 and GD2. (a) Alignment error of GD1 with different scale factor α. (b) Alignment error of GD1 ($\alpha = 0.99$) and GD2.

GD1 with different scale factor α, as represented by (40). It is clear that the horizontal error of original GD1 method ($\alpha = 0.5$) is the largest among these scale factors. As we expected, the horizontal errors caused by IMU biases are significantly suppressed by choosing a larger α, which is more effective to decrease the weight of attitude errors caused by gyroscope bias. However, we cannot completely ignore the weight of gyroscope bias in (40), as the measurements from the gyroscope are indispensable to determine the yaw angle. We will investigate the effect of the scale factor α on improving the attitude accuracy and the principle of choosing α in our future research.

According to Fig.5(b) and Table 1, the horizontal attitudes of GD2 are "insensitive" to the changes of yaw angle, which is consistent with the results of (42)-(45). On the other hand, though affected by yaw angle, the accuracy of GD1 with $\alpha = 0.99$ is very close to GD2 method, which testifies that the method with a larger α (α<1) in (40) is effective to decrease the horizontal attitude errors, as we analyzed in Section III.

Thirdly, simulation is also implemented to compare the alignment accuracy of GD2 method with several popular stationary alignment methods, O-TRIAD [21], ON-TRIAD [21] and AEA method [25]. In the simulation, the yaw angle varies from $0° \sim 360°$ with fixed pitch and roll angle ($10°$, $10°$).

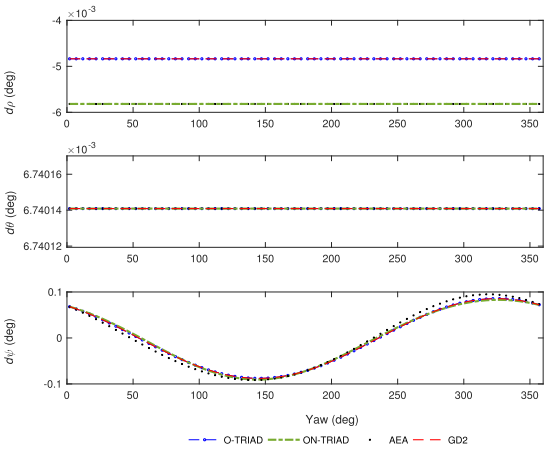

FIGURE 6. Alignment error comparisons of O-TRIAD, ON-TRIAD, AEA and GD2.

TABLE 2. RMSs of O-TRIAD, ON-TRIAD, AEA and GD2 errors.

Methods	$d\rho$ (deg)	$d\theta$ (deg)	$d\psi$ (deg)
O-TRIAD	$4.84e^{-3}$	$6.74e^{-3}$	$6.13e^{-2}$
ON-TRIAD	$5.82e^{-3}$	$6.74e^{-3}$	$6.13e^{-2}$
AEA	$5.82e^{-3}$	$6.74e^{-3}$	$6.59e^{-2}$
GD2	$4.84e^{-3}$	$6.74e^{-3}$	$6.13e^{-2}$

Moreover, the alignment errors of O-TRIAD, ON-TRIAD, AEA and GD2 methods are presented in Fig.6, and the RMS errors of their alignment results are shown in Table 2. Fig.7 denotes the error of the alignment results of GD2 with respect to AEA, O-TRIAD and ON-TRIAD method, respectively.

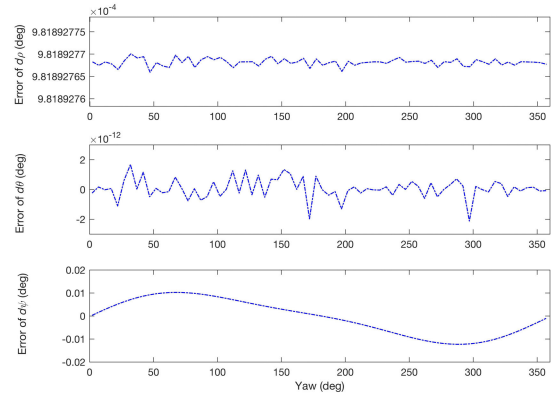

(a)

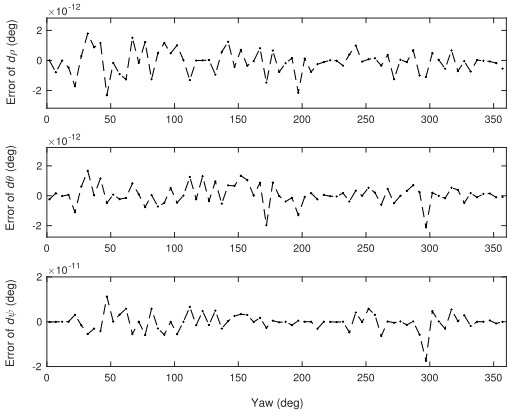

(b)

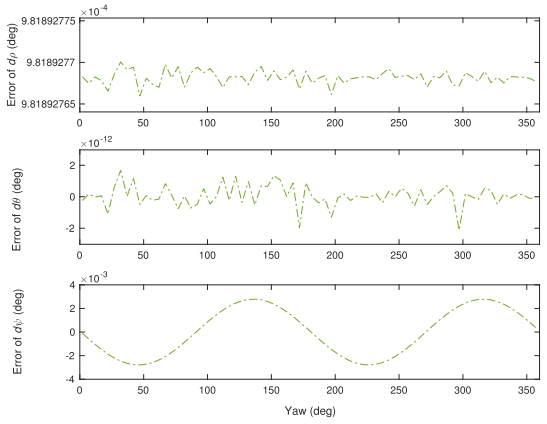

(c)

FIGURE 7. Attitude error of GD2 with respect to AEA, O-TRIAD and ON-TRIAD. (a) Error between GD2 and AEA. (b) Error between GD2 and O-TRIAD. (c) Error between GD2 and ON-TRIAD.

As the basic idea and the attitude expression of GD2 are close to and AEA method, we firstly analyze the alignment results of GD2 with respect to AEA method.

In Fig.6 and Fig.7(a), the deviation of $d\rho$ between GD2 and AEA method is caused by the quaternion normalization of GD2 method, which is the second term in (42) and cannot be ignored in some applications. Additionally, it demonstrates that the normality error of quaternion is also helpful to decrease the pitch error caused by sensor biases in some situations. Secondly, the roll error $d\theta$ of GD2 and AEA equals to each other, as shown in Fig.7(a) and Table 2, which also verifies the result of (45). According to Table 2, the yaw RMS error of GD2 is smaller than that of AEA method in terms of the range of yaw angle $0° \sim 360°$, which demonstrates that the normality error of quaternion and the estimate error of latitude caused by IMU biases can decrease the yaw error to some extent.

According to Fig.6, Fig.7(b) and Table 2, we notice that the alignment result of GD2 method equals to that of the O-TRIAD method, which is an important discovery in the simulation. Additionally, compared with O-TRIAD method, GD2 can be applied to any stationary field alignment without using the latitude information, which is more autonomous and flexible for the practical application. In view of Fig.6 and Table 2, the roll error of GD2 is equal to ON-TRIAD, but its pitch error is slightly smaller than the latter. From Fig.7(c) and Table 2, the yaw error of GD2 with respect to ON-TRIAD varies in the form of persistent amplitude "sine" curve, and the yaw RMS error of GD2 is equal to ON-TRIAD in the range of yaw angle $0° \sim 360°$.

Moreover, we also compare GD2 with the optimization-based alignment (OBA) method [29], which uses quaternion vector to represent the attitude. As OBA method requires several measurements from different instants to determine the attitude, we only consider the initial attitude $(10°, 10°, 45°)$ and $(10°, 10°, 135°)$ in the simulation, of which the duration is 300 seconds. As illustrated by Fig.8, the alignment errors of GD2 are constant values, but the alignment errors of OBA grow with run-time. Besides, the local latitude information is required for OBA method to determine the attitude. Thus, compared with OBA, GD2 is more competent for stationary SINS alignment.

B. EXPERIMENT RESULTS

In this section, a static experiment of fiber optic gyroscope (FOG)-based SINS developed by out lab is performed on a three-axis turntable, as shown in Fig.9. The FOG-based SINS consists of a three-axis accelerometer and a three-axis gyroscope, and its sampling rate is 100 Hz. Their specifications are $100\mu g$ for the accelerometer bias and $0.01°/h$ for the gyroscope bias respectively, as shown in Table 3. The experiment is carried out at Harbin, and local latitude is 45.7347°. Besides, the turntable attitude is set as $(0°, 0°, 315°)$. However, due to the mechanical wear for a long time usage and the dead zone of the mechanical rotational parts, the actual attitude of turntable may not achieve the set value accurately. Additionally, the test data are preprocessed by averaging the raw data from IMU to reduce the distances of sensor noises.

The alignment results of O-TRIAD, ON-TRIAD, AEA and GD2 in the static experiment are presented in Fig.10, Table 4 and Table 5. Fig.10 (a) denotes the alignment results and Fig.10 (b) denotes their corresponding alignment errors. From Fig.10, we observe that the alignment

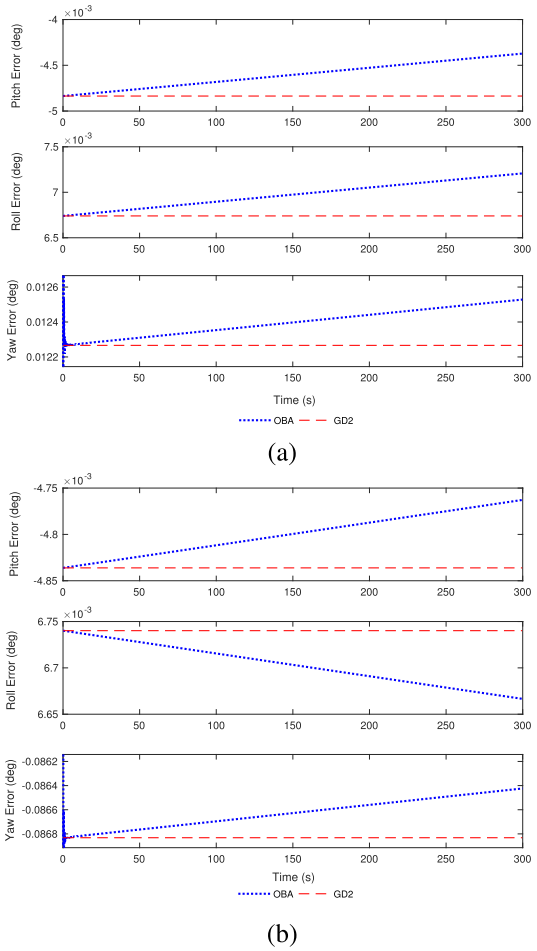

FIGURE 8. Alignment errors of OBA and GD2 at different initial attitude. (a) (10°, 10°, 45°). (b) (10°, 10°, 135°) .

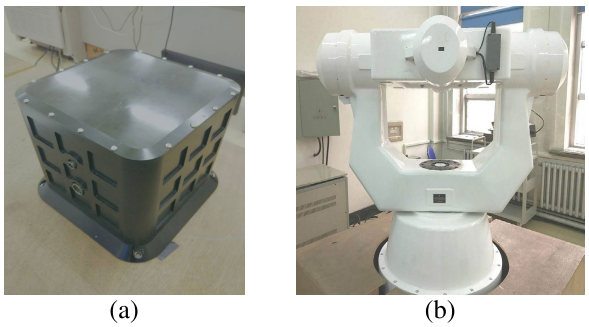

FIGURE 9. Static experiment of FOG-based SINS on turntable. (a) FOG-based SINS. (b) Three-axis turntable .

TABLE 3. High precision IMU specifications.

Parameters	Gyroscope	Accelerometer
Sensor bias	$0.01°/h$	100μg
Scale factor	20ppm	30ppm
Dynamic range	$\pm 150°/h$	± 20 g
Random walk	$0.001°/\sqrt{h}$	—

results of O-TRIAD, ON-TRIAD, AEA and GD2 are close to each other in the static experiment. From Table 4, we notice that both the horizontal errors and yaw error of

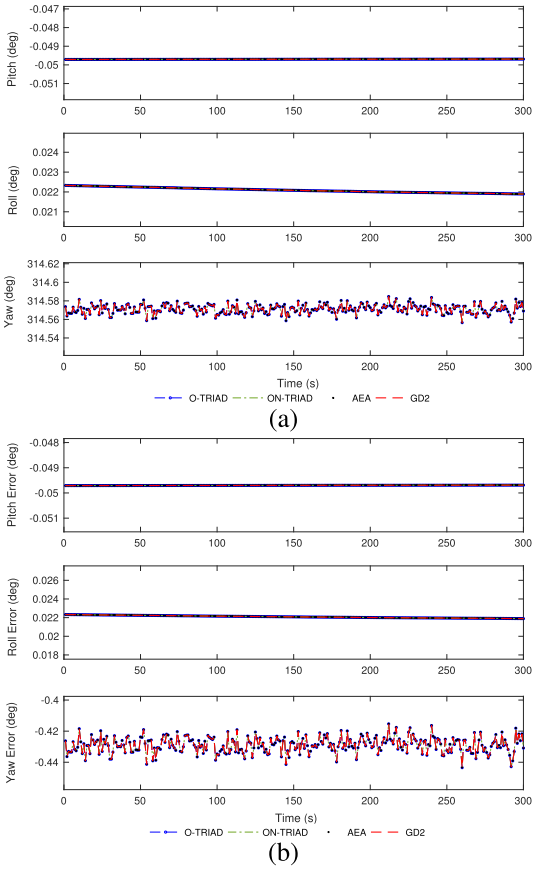

FIGURE 10. Alignment result comparisons of O-TRIAD, ON-TRIAD, AEA and GD2. (a) Alignment results. (b) Alignment errors.

TABLE 4. RMSs of O-TRIAD, ON-TRIAD, AEA and GD2 errors.

Methods	$d\rho$ (deg)	$d\theta$ (deg)	$d\psi$ (deg)
O-TRIAD	$4.97e^{-2}$	$2.21e^{-2}$	4.29^{-1}
ON-TRIAD	$4.97e^{-2}$	$2.21e^{-2}$	4.29^{-1}
AEA	$4.97e^{-2}$	$2.21e^{-2}$	4.29^{-1}
GD2	$4.97e^{-2}$	$2.21e^{-2}$	4.29^{-1}

TABLE 5. SDs of O-TRIAD,, ON-TRIAD, AEA and GD2 errors.

Methods	$d\rho$ (deg)	$d\theta$ (deg)	$d\psi$ (deg)
O-TRIAD	$5.43e^{-6}$	$1.26e^{-4}$	5.06^{-3}
ON-TRIAD	$5.48e^{-6}$	$1.26e^{-4}$	5.05^{-3}
AEA	$5.48e^{-6}$	$1.26e^{-4}$	5.06^{-3}
GD2	$5.42e^{-6}$	$1.26e^{-4}$	5.06^{-3}

the attitude are larger than the theoretical analysis results in Fig.6 and Table 2, especially the yaw error is about 0.429° with respective to the simulation result 0.0613°. Furthermore, we also analyze the standard deviations (SDs) of O-TRIAD, ON-TRIAD, AEA and GD2 in Table 5 which indicates their alignment results are steady around (0.0497°, 0.0221°, 314.571°). In fact, the alignment errors of O-TRIAD, ON-TRIAD, AEA and GD2 in the static

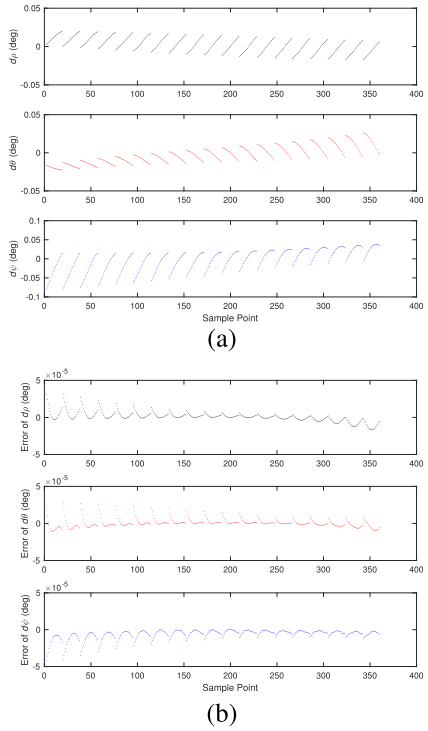

FIGURE 11. Estimated attitude error (a) and the residual of estimated error (b) of GD1.

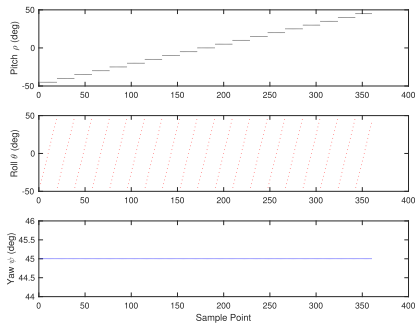

FIGURE 12. The actual attitude with varying pitch and roll angle.

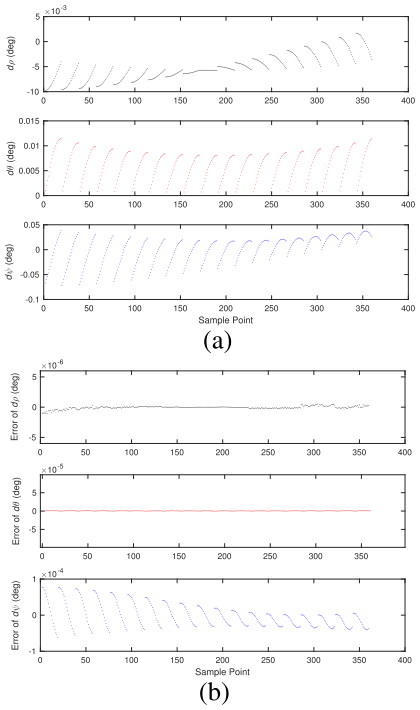

FIGURE 13. Estimated attitude error (a) and the residual of estimated error (b) of GD2.

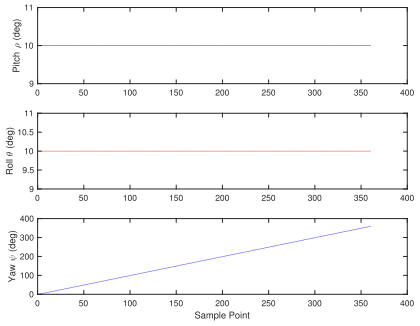

FIGURE 14. The actual attitude with varying yaw angle.

experiment are mainly caused by the dead zone of the mechanical rotational parts for a long time usage. More importantly, GD2 can achieve an alignment accuracy as good as O-TRIAD, without using the priori local latitude information, which is more autonomous and flexible for many field applications.

V. CONCLUSION

In this paper, SINS self-alignment on the stationary base is formulated as an optimization problem, and two gradient descent (GD) optimization-based self-alignment methods (GD1 and GD2) are proposed to determine the initial attitude in real time. Different from conventional alignment methods, GD1 constructs a quaternion-based objective function for stationary SINS, and employs GD optimization to achieve the minimum of the objective function. Furthermore, GD2 constructs an improved quaternion-based objective function which utilizes the measurements from IMU to represent the Earth rate instead of using the local latitude directly. In addition, we also analyze the bias errors of accelerometer and gyroscope and the quaternion normality error for GD1 and GD2 method respectively. Compared with GD2, the horizontal errors of GD1 are affected by the gyroscope bias, which mainly dominates the alignment errors. Based on the analysis results, a scale factor is also introduced to decrease the alignment error of GD1 caused by gyroscope biases. Simulation and static experiment are implemented to test the performances of GD1 and GD2 method, and the results verify the accuracy and speed of the proposed methods. Compared with O-TRIAD, AEA and OBA, GD2 is more competent for SINS self-alignment when the local latitude information is not available. Besides, compared with OBA, the alignment errors of GD2 don't grow with run-time. Compared with ON-TRIAD, GD2 can also achieve better alignment accuracy

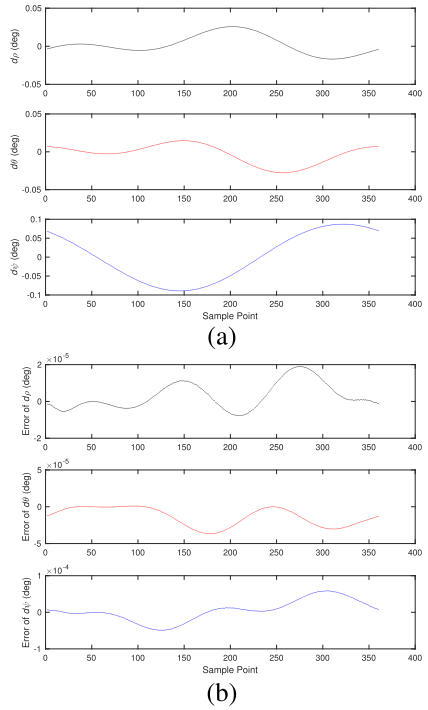

FIGURE 15. Estimated attitude error (a) and the residual of estimated error (b) of GD1.

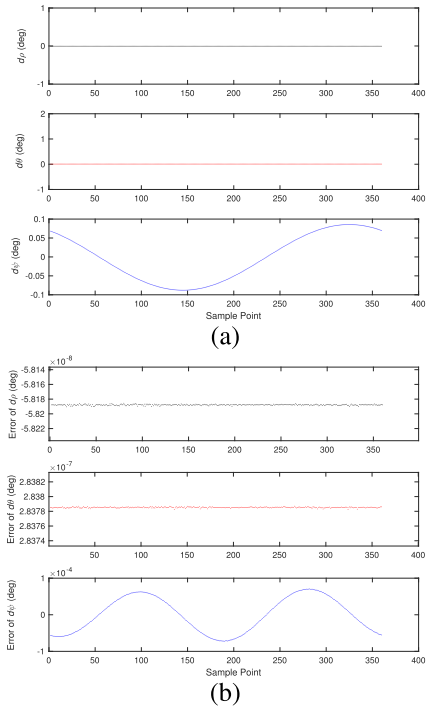

FIGURE 16. Estimated attitude error (a) and the residual of estimated error (b) of GD2.

in many cases, though their yaw RMS errors are equal in the range of yaw angle $0^\circ \sim 360^\circ$. Moreover, the simulation results in the Appendix prove the conclusions of the error analysis of GD1 and GD2 methods.

APPENDIX

In this section, simulations are implemented to illustrate the validity of error analysis results of GD1 and GD2 method in Section III. In the first set of simulation, pitch and roll angle vary from $-45^\circ \sim 45^\circ$, respectively, and the yaw angle is a fixed angle $\psi = 45^\circ$, as demonstrated by Figs. 11-13. In the second set of simulation, the yaw angle varies from $0^\circ \sim 360^\circ$, and pitch and roll angle are fixed angles ($\rho = 10^\circ, \theta = 10^\circ$), as denoted by Figs. 14-16.

In Fig.11 and Fig.15, Figure (a) denotes the estimated attitude error of GD1 method and Figure(b) represents the corresponding residual of the attitude error model of GD1 method in (38). In Fig.13 and Fig.16, Figure(a) denotes the estimated attitude error of GD2 method, and Figure(b) not only represents the corresponding residual of the attitude error model of GD2 method in (42)-(43), but also demonstrate the error of the attitude model in (41). As the objective function of GD2 is a standard convex function, numerical results illustrate that (41) is the optimal solution for minimizing the objective function.

Compared with the estimated attitude errors on Figure (a) of Fig. 11 and Figs. 13-16, the residuals of the estimated attitude error on Figure (b) can be ignored, which illustrates that the error models in (38) and (42)-(43) can correctly reflect the changes of GD1 and GD2 method.

REFERENCES

[1] K. R. Britting, *Inertial Navigation Systems Analysis*. New York, NY, USA: Wiley, 1971.
[2] X. Liu, Y. Zhao, X. Liu, Y. Yang, Q. Song, and Z. Liu, "An improved self-alignment method for strapdown inertial navigation system based on gravitational apparent motion and dual-vector," *Rev. Sci. Instrum.*, vol. 85, no. 125108, pp. 1–11, 2014.
[3] B. Liu, S. Wei, J. Lu, J. Wang, and G. Su, "Fast self-alignment technology for hybrid inertial navigation systems based on a new two-position analytic method," *IEEE Trans. Ind. Electron.*, vol. 67, no. 4, pp. 3226–3235, Apr. 2020.
[4] F. Li, J. Xu, and H. He, "Backtracking velocity denoising based autonomous in-motion initial alignment," *IEEE Access*, vol. 6, pp. 67144–67155, Oct. 2018.
[5] Y. Che, Q. Wang, W. Gao, and F. Yu, "An improved inertial frame alignment algorithm based on horizontal alignment information for marine SINS," *Sensors*, vol. 15, no. 10, pp. 25520–25545, Oct. 2015.
[6] X. Xu, J. Lu, and T. Zhang, "A fast-initial alignment method with angular rate aiding based on robust Kalman filter," *IEEE Access*, vol. 7, pp. 51369–51378, Apr. 2019.
[7] L. Chang, J. Li, and K. Li, "Optimization-based alignment for strapdown inertial navigation system: Comparison and extension," *IEEE Trans. Aerosp. Electron. Syst.*, vol. 52, no. 4, pp. 1697–1713, Aug. 2016.
[8] T. Du, C. Tian, J. Yang, S. Wang, X. Liu, and L. Guo, "An autonomous initial alignment and observability analysis for SINS with bio-inspired polarized skylight sensors," *IEEE Sensors J.*, vol. 20, no. 14, pp. 7941–7956, Jul. 2020.
[9] F. O. Silva, E. M. Hemerly, and W. C. L. Filho, "Error analysis of analytical coarse alignment formulations for stationary SINS," *IEEE Trans. Aerosp. Electron. Syst.*, vol. 52, no. 4, pp. 1777–1796, Aug. 2016.
[10] W. Huang and M. Li, "A self-alignment method of MEMS biaxial rotation modulation strapdown compass for marine applications," *IEEE Access*, vol. 7, pp. 151595–151609, Oct. 2019.
[11] J. Li, W. Gao, and Y. Zhang, "Gravitational apparent motion-based SINS self-alignment method for underwater vehicles," *IEEE Trans. Veh. Technol.*, vol. 67, no. 12, pp. 11402–11410, Dec. 2018.
[12] J. Wang, T. Zhang, J. Tong, and Y. Li, "A fast SINS self-alignment method under geographic latitude uncertainty," *IEEE Sensors J.*, vol. 20, no. 6, pp. 2885–2894, Mar. 2020.

[13] H. Yang, B. Zhou, L. Wang, Q. Wei, and R. Zhang, "A novel method for fast stationary initial alignment based on extended measurement information," *IEEE Access*, vol. 7, pp. 165873–165883, Nov. 2019.
[14] J. Cheng Fang and D. Jun Wan, "A fast initial alignment method for strapdown inertial navigation system on stationary base," *IEEE Trans. Aerosp. Electron. Syst.*, vol. 32, no. 4, pp. 1501–1504, Oct. 1996.
[15] Z. Chuanbin, T. Weifeng, and J. Zhihua, "A novel method improving the alignment accuracy of a strapdown inertial navigation system on a stationary base," *Meas. Sci. Technol.*, vol. 15, no. 4, pp. 765–769, Mar. 2004.
[16] A. Acharya, S. Sadhu, and T. K. Ghoshal, "Improved self-alignment scheme for SINS using augmented measurement," *Aerosp. Sci. Technol.*, vol. 15, no. 2, pp. 125–128, Mar. 2011.
[17] D. Chung, J. Gyu Lee, C. Gook Park, and H. Won Park, "Strapdown INS error model for multiposition alignment," *IEEE Trans. Aerosp. Electron. Syst.*, vol. 32, no. 4, pp. 1362–1366, Jun. 1996.
[18] I. Rhee, M. F. Abdel-Hafez, and J. L. Speyer, "Observability of an integrated GPS/INS during maneuvers," *IEEE Trans. Aerosp. Electron. Syst.*, vol. 40, no. 2, pp. 526–535, Apr. 2004.
[19] J. Xiong, H. Guo, and Z. H. Yang, "A two-position SINS initial alignment method based on gyro information," *Adv. Space Res.*, vol. 53, no. 11, pp. 1657–1663, Jun. 2014.
[20] C. Tan, X. Zhu, Y. Su, Y. Wang, Z. Wu, and D. Gu, "A new analytic alignment method for a SINS," *Sensors*, vol. 15, no. 11, pp. 27930–27953, Nov. 2015.
[21] Y. Fuh Jiang, "Error analysis of analytic coarse alignment methods," *IEEE Trans. Aerosp. Electron. Syst.*, vol. 34, no. 1, pp. 334–337, Jan. 1998.
[22] M. D. Shuster, "A survey of attitude representations," *Navigation*, vol. 8, no. 9, pp. 439–517, 1993.
[23] P. G. Savage, "Strapdown inertial navigation integration algorithm design part I: Attitude algorithms," *J. Guid. Control Dyn.*, vol. 21, no. 1, pp. 19–28, Jan. 1998.
[24] R. Mahony, T. Hamel, and J.-M. Pflimlin, "Nonlinear complementary filters on the special orthogonal group," *IEEE Trans. Autom. Control*, vol. 53, no. 5, pp. 1203–1218, Jun. 2008.
[25] J. Li, J. Fang, and M. Du, "Error analysis and gyro-bias calibration of analytic coarse alignment for airborne POS," *IEEE Trans. Instrum. Meas.*, vol. 61, no. 11, pp. 3058–3064, Nov. 2012.
[26] H. Zhao, H. Shang, Z. Wang, and M. Jiang, "Comparison of initial alignment methods for SINS," in *Proc. 9th World Congr. Intell. Control Autom.*, Taipei, China, Jun. 2011, pp. 42–47.
[27] F. O. Silva, E. M. Hemerly, and W. C. L. Filho, "Influence of latitude in coarse self-alignment of strapdown inertial navigation systems," in *Proc. IEEE/ION Position, Location Navigat. Symp. (PLANS)*, Monterey, CA, USA, May 2014, pp. 1219–1226.
[28] M. D. Shuster and S. D. Oh, "Three-axis attitude determination from vector observations," *J. Guid. Control*, vol. 4, no. 1, pp. 70–77, Jan. 1981.
[29] M. Wu, Y. Wu, X. Hu, and D. Hu, "Optimization-based alignment for inertial navigation systems: Theory and algorithm," *Aerosp. Sci. Technol.*, vol. 15, no. 1, pp. 1–17, Jan. 2011.
[30] S. Ruder, "An overview of gradient descent optimization algorithms," 2016, *arXiv:1609.04747*. [Online]. Available: http://arxiv.org/abs/1609.04747
[31] J. Solà, "Quaternion kinematics for the error-state Kalman filter," 2017, *arXiv:1711.02508*. [Online]. Available: http://arxiv.org/abs/1711.02508
[32] S. O. H. Madgwick, A. J. L. Harrison, and R. Vaidyanathan, "Estimation of IMU and MARG orientation using a gradient descent algorithm," in *Proc. IEEE Int. Conf. Rehabil. Robot.*, Zurich, Switzerland, Jun. 2011, pp. 1–7.
[33] Y. Yuan, "A new stepsize for the steepest descent method," *J. Comput. Math.*, vol. 24, no. 2, pp. 149–156, 2006.
[34] J. Duchi, E. Hazan, and Y. Singer, "Adaptive subgradient methods for online learning and stochastic optimization," *J. Mach. Learn. Res.*, vol. 12, pp. 2121–2159, Feb. 2011.

JINGCHUN LI was born in 1988. He received the M.S. degree from Harbin Engineering University, Harbin, China, in 2015, and the Ph.D. degree in instruments science and technology from the Harbin Institute of Technology, Harbin, in 2020.

He is currently working as a Postdoctoral Researcher with the Peng Cheng Laboratory, Shenzhen, China. His research interests include signal processing, inertial navigation systems, and multi-UAV cooperative navigation and control.

JIACHONG CHANG was born in 1993. He received the B.S. degree from the Department of Automation, Harbin Engineering University, Harbin, China, in 2016, and the M.S. degree from the Harbin Institute of Technology, Harbin, in 2018, where he is currently pursuing the Ph.D. degree in instruments science and technology.

His current research interests include strapdown inertial navigation systems and fault diagnosis technology.

YA ZHANG was born in 1987. She received the B.S. and Ph.D. degrees from the Department of Automation, Harbin Engineering University, Harbin, China, in 2010 and 2015, respectively.

She is currently a Postdoctoral Researcher with the School of Electrical Engineering and Automation, Harbin Institute of Technology. Her current research interests include strapdown inertial navigation technology, initial alignment algorithms, and integration navigation technology.